Chapter

Free-electron Driven Terahertz Wave Sources Based on Simth-Purcell Effect

Weihao Liu, Zijia Yu and Zhi Tao

Abstract

Terahertz electromagnetic wave is one of the hottest research topics in nowadays scientific world thanks to its broad applications in material characterization, medical imaging, wireless communication, and security checking etc. Using free-electron beams to interact with periodic structures via the famous Smith-Purcell effect is an efficient way of generating high-power terahertz radiation. In this chapter, we introduce the basic theory and latest developments of the terahertz radiation schemes using a free-electron beam (including continuous electron beam, a single electron bunch, and a train of electron bunches, etc.) to interact with periodic electromagnetic structures, including grating, surface plasmonics, and subwavelength hole arrays, via a special Smith-Purcell effect or Cherenkov-like effect. A kind of free-electron lasers based on the special Smith-Purcell radiation in the terahertz region is proposed and investigated, which can be developed as high-power terahertz wave sources for practical applications.

Keywords: Terahertz, free-electron beam, beam-wave interaction, diffraction radiation

1. Introduction

Terahertz electromagnetic wave is an attractive topic to researchers thanks to its broad application prospects in fields as diverse as biological imaging, materials science, and astrophysics [1]. However, the development of compact, high-power, broadly tunable terahertz sources is challenging [2, 3]. Compared with other kinds of terahertz sources, the free-electron driven sources, such as conventional vacuum electron devices (VEDs) [4] and free electron lasers (FELs) [5], can generate electromagnetic radiation with high power and desirable coherence. However, VEDs can hardly reach the frequency as high as 1 THz and FELs require tremendous costs and cumbersome peripheral equipment. The radiation sources based on the Smith–Purcell radiation (SPR) [6] can avoid the disadvantages of both VEDs and FELs, affording promising ways for developing compact terahertz sources [7–11].

Since its first experimental observation in 1953, Smith–Purcell radiation (SPR), which is generated when a uniformly moving electron beam passes over a periodic surface, has been an attractive research topic for its applications in radiation generation, beam acceleration and nondestructive particle diagnostics etc. [6, 12–15]. It is characterized by the following well-known dispersion relation:

$$\lambda = -\frac{L}{n}\left(\frac{1}{\beta} - \cos\theta\right), \tag{1}$$

where λ is the radiation wavelength, θ the radiation direction, L the structural period, β the ratio of the beam velocity to the speed of light, and n a negative integer indicating the harmonic order.

Unfortunately, the efficiency of conventional SPR in practice is usually not high enough, which restricts the power and efficiency of the terahertz generating sources based on it [16]. Enhancing the efficiency of SPR will substantially improve the performances of the related terahertz sources. Developing new mechanisms or radiation schemes to improve the efficiency and power of SPR terahertz sources is the major goal of the present chapter, which is organized as follows. In Section 2, we will first introduce a unique kind of SPR, so-called Special Smith-Purcell Radiation (S-SPR), which can enhance the efficiency of SPR. And then several variants of S-SPR will be proposed and investigated. In Section 3, a kind of terahertz free-electron laser based on the mechanism of S-SPR will be illustrated, which can generate terahertz radiation with higher power than ordinary SPR devices. Section 4 concludes this chapter.

2. Special Smith-Purcell radiation (S-SPR)

Traditionally, there are two theoretical models dealing with the mechanism of SPR. The first one is the diffraction model [17, 18], by which SPR is considered as the diffraction of the periodic surface to the evanescent self-field of an electron beam. The other one is the surface-current model based on the image-charge approximation [19, 20], according to which SPR is generated from the surface-current, induced by a moving electron beam, on the periodic metallic structure. Both models can deduce the SPR relation.

In the past years, we revealed a class of S-SPR, which cannot be perfectly involved in the previous theoretical models mentioned above. We have found that it is generated due to the coherent interference of the radiation from an one-dimensional or two-dimensional array of resonant modes [21–23]. In this section, a series of variants of S-SPR are proposed and investigated.

2.1 S-SPR from one-dimensional gratings

Figure 1 shows one of the schemes that we are going to study. At first sight, it is a rectangular optical grating that is commonly used in ordinary SPR (O-SPR). For comparison purpose, let us first briefly visit O-SPR. According to the diffraction

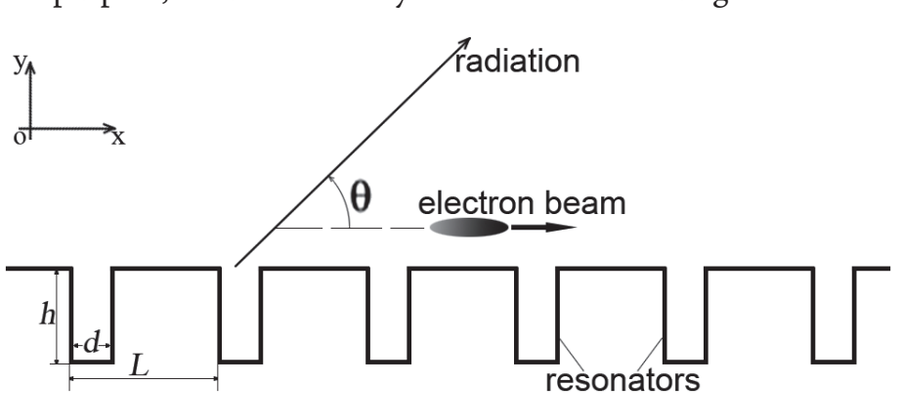

Figure 1.
Schematic diagram of the special Smith–Purcell radiation from the resonator array.

model, the diffraction waves from a grating consist both surface waves and radiation waves. The surface waves, the frequencies of which are below the threshold of SPR, can only propagate along the grating and cannot radiate except for the abrupt change of structure [24, 25], and the radiation waves, which are the negative harmonics of diffraction, can radiate into the upper half-space, and the dependence of radiation frequency on direction satisfies Eq. (1) [26]. In other words, the surface waves and radiation waves are independent from each other: the surface waves are bound to the periodic structure while the radiation waves extend to all directions in the upper half-space, as shown by the simulated results given in **Figure 2(a)**. The simulated radiation spectrum, shown in **Figure 2(b)**, covers a wide frequency band, which is because the radiation direction is continuously changing while the electron beam is moving. **Figure 2(c)** shows that the frequency of the surface wave is below the threshold of SPR.

Now we reduce the gap width d (all other parameters are kept unchanged, this simulated results are given in **Figure 3**, which shows that the radiation spectrum becomes a narrow band one and the spectrum density is 1.5 times enhanced, see **Figure 3(b)**. In addition, the radiation is almost focused at a specific direction defined by Eq. (1), see **Figure 3(a)**. Hence, we obtain a special kind of SPR with monochromatic spectrum and with enhanced intensity at the specific direction determined by SPR relation, which is exactly the S-SPR that will be discussed in the following.

As is known that the surface waves on a periodic structure are formed by the coupling of resonator modes in the periodic resonator array [27, 28]. When we reduce the gap width d, the distance between the adjacent resonators will be increased, which will obviously weaken the coupling of the resonator modes. The surface waves will no longer exist when the coupling of the resonator modes are eliminated. Under this circumstance, the grating changes into an array of independent resonators. Following the above analysis, the mechanism of S-SPR can then be stated as follows. As an electron beam skims over the resonator array, the resonant modes in the array will be excited one by one. These resonant modes then generate radiation through the apertures one after another. And the radiation frequencies are just the eigenfrequencies of the resonator modes. In the direction given by Eq. (1), the phase shift from every adjacent resonator is $2n\pi$ (n is a integer), indicating that the radiation from all resonators is coherent. So as that the radiation in this direction will be enhanced, while in all other directions the radiations from different resonators will counteract each other, and the radiation cannot occur. This is just what have been shown in **Figure 3**.

The resonator modes play an essential role in S-SPR since they determine both radiation frequency and direction. For the case that the gap width is much less than the radiation wavelength ($\lambda \ll d$), the radiations are largely from the transverse electromagnetic (TEM) modes of resonators. To estimate the eigenfrequencies of these modes, we make the approximation thatE_x reaches a maximum at the aperture of the groove, so as that theE_x distributions in the resonator can be illustrated by **Figure 4**, based on which the oscillation wavelength λ of the resonator modes can be expressed by:

$$\lambda = h/\left(\frac{m}{2} + \frac{1}{4}\right) \tag{2}$$

where m is a non-negative integer, indicating the mode number, and h is the depth of the groove (resonator).

To realize S-SPR, the following conditions should be satisfied. 1) The period L and gap width d should be well matched to prevent the coupling of electromagnetic

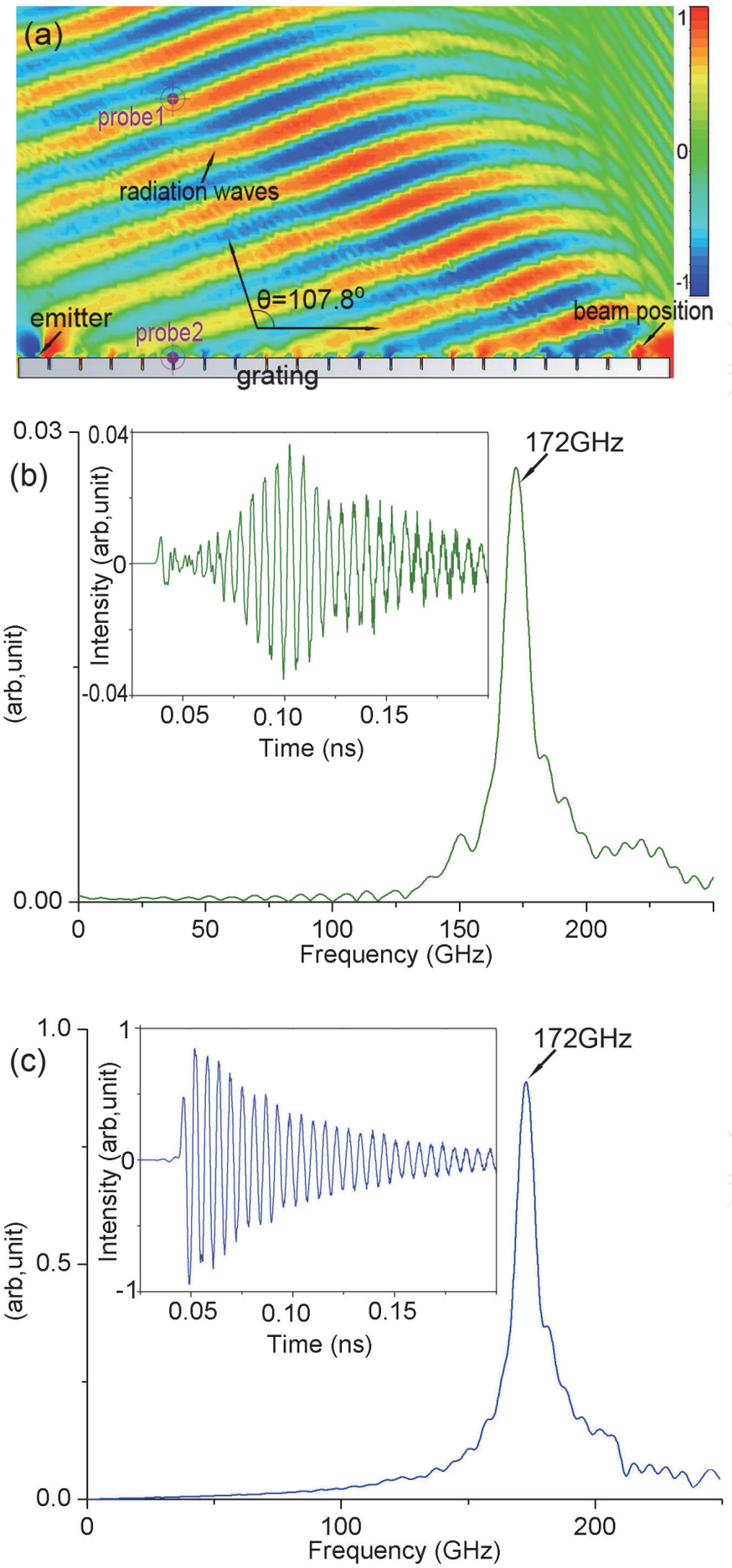

Figure 2.
(a) Simulated contour map of the E_x field of the O-SPR. (b) Simulated radiation spectrum and the waveform in the time-domain. (c) Simulated spectrum of the surface waves and the waveform in the time-domain.

modes in adjacent resonators. Namely, the resonators are deep-narrow-rectangular grooves (DNRGs). 2) The depth of the resonators should be neither too small, otherwise the resonator modes cannot be effectively excited, nor be too large,

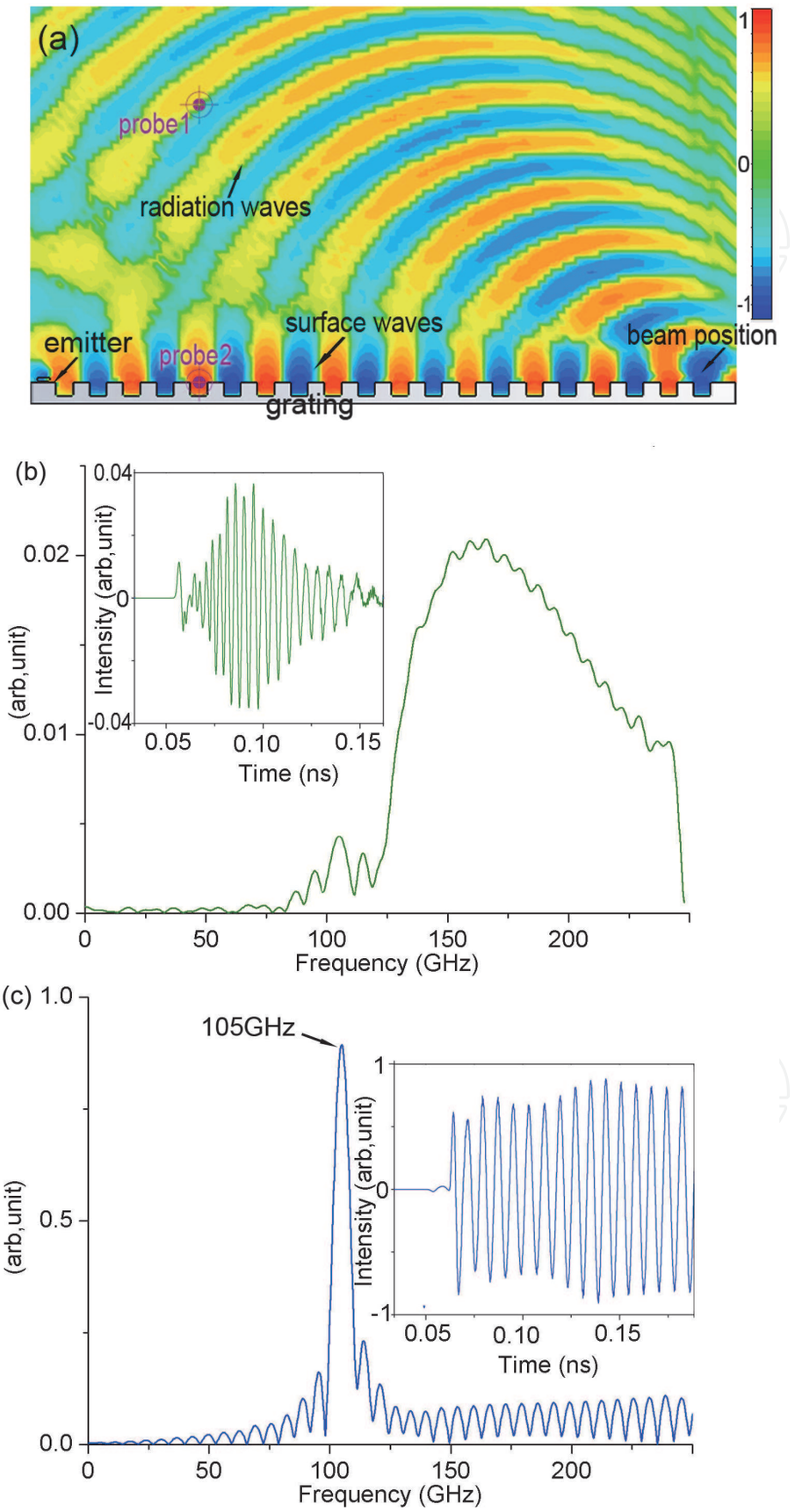

Figure 3.
(a) Simulated contour map of the E_x field of S-SPR. (b) Simulated radiation spectrum and the waveform in the time-domain. (c) Simulated spectrum of the surface waves and the waveform in the time-domain.

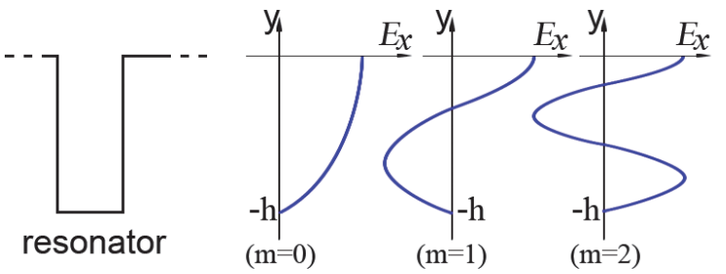

Figure 4.
Diagram of a single resonator and the distribution of the E_x component in the y direction for three resonator modes.

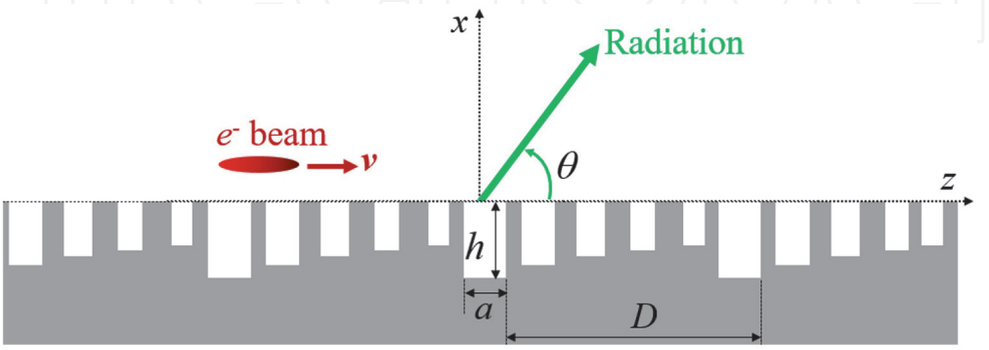

Figure 5.
Diagram of the free-electron beam exciting an array of DNRG-clusters with gradient sizes.

otherwise the SPR cannot be realized since the frequency is below the SPR threshold. 3) The frequency of resonator modes, the grating period, and the beam velocity should be associated to satisfy the SPR relation.

For the S-SPR from an array of DNRGs, only a single radiation frequency can be efficiently obtained. In order to realize several radiation frequencies simultaneously, namely to get multi-color radiation, we proposed to a scheme in which every unit of the array consists several DNRGs with different sizes (gradient DNRGs) as shown in **Figure 5** [29]. The radiation from different DNRGs cannot be coherent since their resonant frequencies are different, however, the radiation from all DNRGs of the same shape in the array will be coherent, which is exactly the S-SPR illustrated above. Thus, we can get an improved S-SPR, which has multiple radiating frequencies. The DNRGs with different shapes will radiate different frequencies at different directions (θ_i). So as that, by using the gradient DNRGs, the spectrum of SPR can be discretized to be a series of peak frequencies with enhanced intensities. Not only spectrum is discretized, but also the radiation directions are also discretized as shown in **Figure 6**. By integrating the field energy in the spectrum band, we obtain that the total radiation intensity is enhanced by more than an order of magnitude.

In the S-SPR illustrated above, all the DNRGs have high aspect-ratios with h/a>20. The manufacturing of the metal structures with high aspect-ratios in the terahertz region is a challenge in practices. In addition, the energy capacities of such grooves/holes are essentially restricted by the structure volume, which reduces the efficiency of terahertz emission and manipulation. We find that, for a single groove with a small aspect-ratio, the field has a broad spectrum. In contrast, for the coupled grooves, the spectrum shows the feature of resonance: having a sharp peak resonating frequency and a narrow bandwidth, see **Figure 7**. As the number of groove (N_g) increases, the peak becomes sharper and the spectrum bandwidth becomes narrower [30]. In other words, a cluster of grooves can operate as an effective electromagnetic resonator, holding a series of Fabry–Pérot (FP)-like modes.

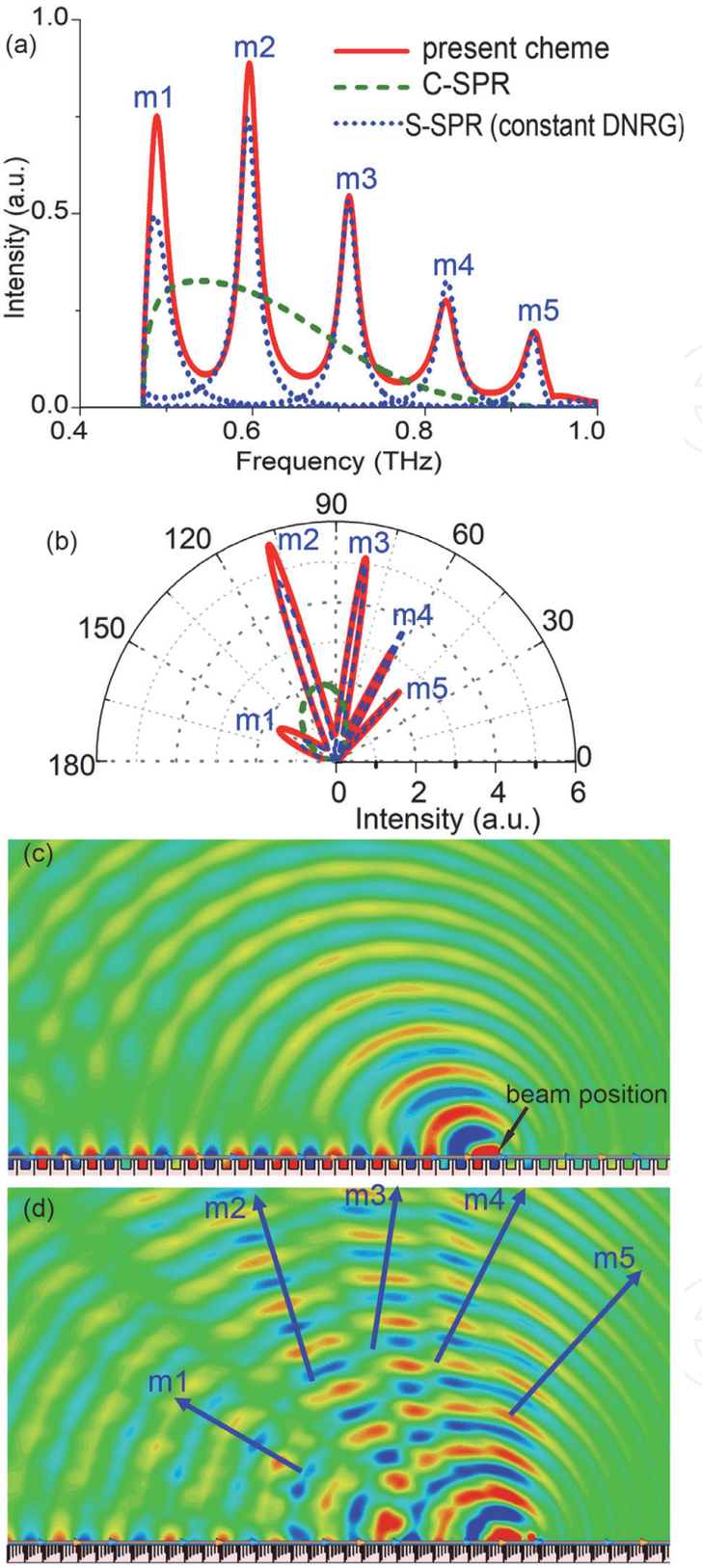

Figure 6.
(a) Calculated radiation spectra of the SPR from an array of gradient DNRGs (present scheme), of O-SPR (green dash line), and of S-SPRs with constant size DNRGs (blue dot lines). (b) Calculated angular distribution of the radiation. (c) Simulated E_z contour map in x-z section for the case of C-SPR. (d) Simulated E_z contour map for the case of gradient DNRGs.

The field intensities within the coupled grooves are remarkably higher than that within a single uncoupled groove, indicating that coupled grooves have much higher energy capacity, and can interact with the electron beam more efficiently. From the insets we can see that the electric fields within adjacent grooves are in the

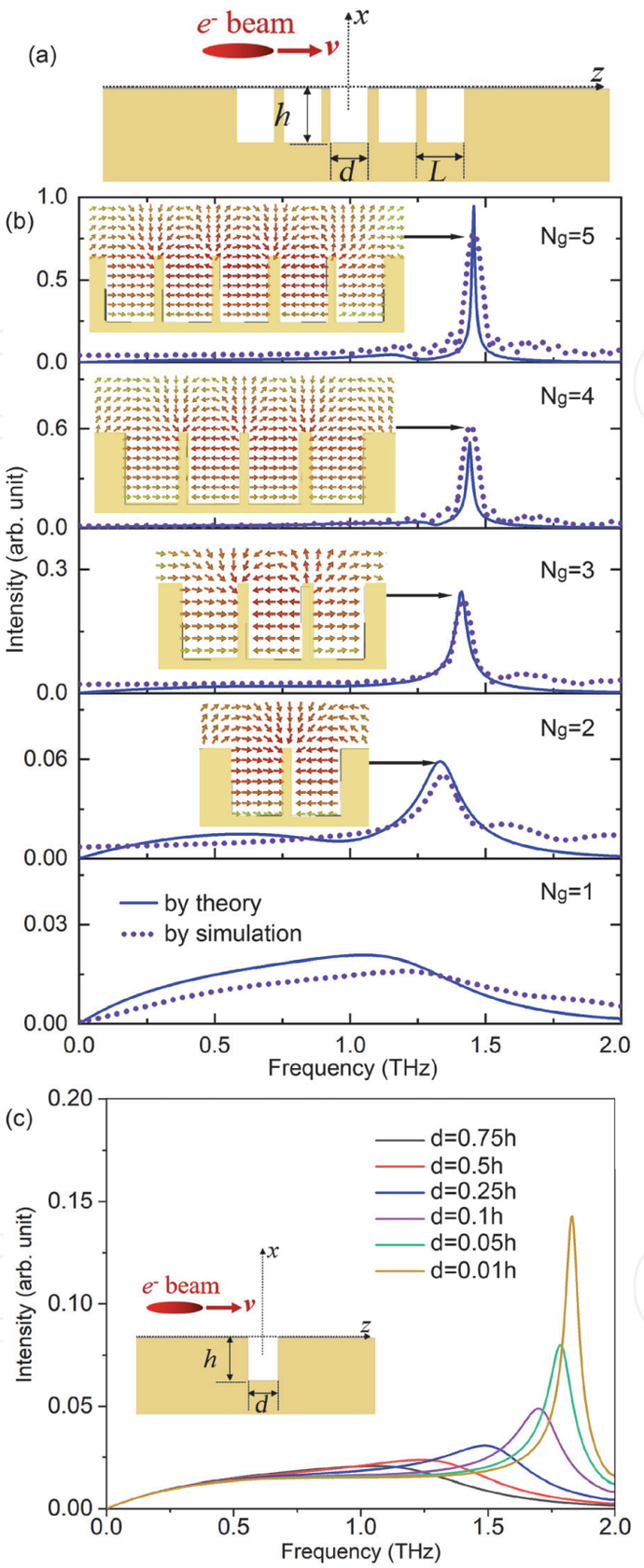

Figure 7.
(a) Schematic diagram of the coupled grooves excited by free-electron beam. (b) Calculated and simulated field spectra at the groove-apertures for different N_g. The insets are simulated snapshots of the electric field distributions.

opposite directions, indicating that the phase difference between adjacent grooves is π. We would refer to this kind of FP resonant mode as π mode.

Based on the above knowledge, we propose to use electron beam to excite an array of coupled grooves, the calculated and simulated results are shown in **Figure 8**. For

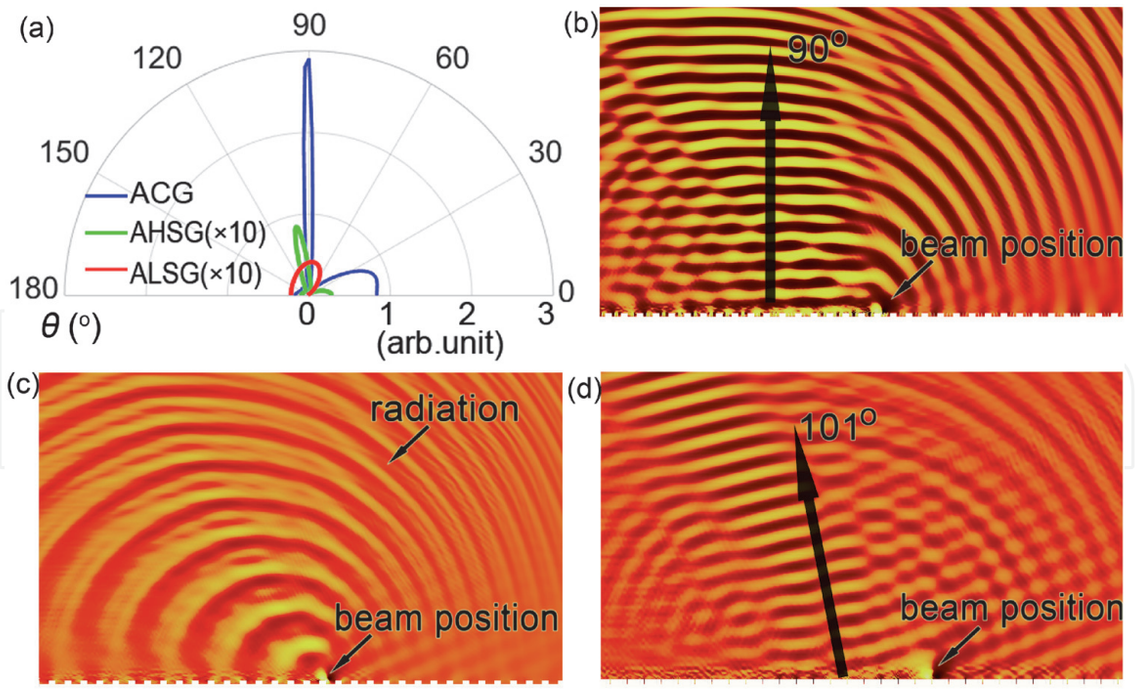

Figure 8.
(a) Calculated angular distribution of radiation from three cases (ACG, ALSG, and AHSG). (b), (c), and (d) are simulated E_z contour-maps for the cases of ACG, ALSG, and AHSG, respectively.

the purpose of comparison, other two cases—an array of low-aspect-ratio single-grooves (ALSG) and an array of high-aspect-ratio single-grooves (AHSG)—are also simulated. For the case of ALSG, the radiation is at all directions, illustrating a typical feature of O-SPR. For AHSG, the radiation is mainly concentrated at a specified direction (θ=101°), indicating the feature of S-SPR [22]. For the proposed array of couple-grooves (ACG), the main radiation wave is at the specified direction (θ = 90°). Here the direction changes due the changing of the period of the array. The figure shows that by using the coupled grooves, the radiation intensity can be enhanced by more than an order of magnitude compared with that from ALSG and AHSG.

2.2 S-SPR from two-dimensional sub-wavelength hole arrays

Sub-wavelength hole array (SHA) is a unique open period structure, which has tremendous interesting properties and applications [31–33]. Here we propose a modified S-SPR by using a sheet FEB to excite two-dimensional (2D) SHAs, see **Figure 9** [34]. The 2D SHA is formed by periodically etching rectangular sub-wavelength holes on a planar conductor plate. All the one-dimensional (1D) SHAs are parallel, and every adjacent two arrays have a certain deviation in the longitudinal (z) direction, forming a parallelogram pattern of holes on the plate. We set the longitudinal width of the hole to be much less than the spatial period of the array ($d \ll \lambda$), such that each hole is an independent resonant unit with specific resonant modes. In light of the shapes and boundary conditions of sub-wavelength holes, the frequencies of the resonant modes can be approximately expressed as:

$$f_{l,m,n} = \frac{c}{2}\sqrt{\left(\frac{l}{d}\right)^2 + \left(\frac{n}{h}\right)^2 + \left(\frac{m}{w}\right)^2} \tag{3}$$

in which h, w and d are the hole parameters shown in **Figure 9**. l, m and p are non-negative integers signifying the mode orders. These resonant modes are

successively excited by the FEB and then generate coherent radiation via S-SPR effect, namely, the radiations from all sub-wavelength holes constructively interfere. The frequency is exactly the frequency of resonant modes defined by Eq. (3), and the radiation direction is determined by SPR relation. Since the 1D SHAs are periodically arranged not only in the longitudinal (z) direction but also in the lateral directions (z' and z" directions shown in the **Figure 9**), the coherent radiation can be realized when the constructive interference is realized at specified directions in the 3D space. **Figure 10** shows the simulated results. When the 2D SHAs are arranged rectangularly ($\alpha_1 = 0$), there is only one dominant radiation direction. As the deviation increases, the radiation gradually deflects to the lateral directions, and two radiation lobes are obtained. Sinceθ_0 can be adjusted by changing beam velocity or structure periodicity (L), the coherent radiation can be steered to any directions in the 3D space.

Since the total radiation is the superposition of all the radiating units in the 2D SHA, high radiation intensity can be obtained by setting a wide FEB together with a large 2D SHA. In addition, since several frequencies are obtained and each frequency component could radiate at several directions, the proposed scheme can be

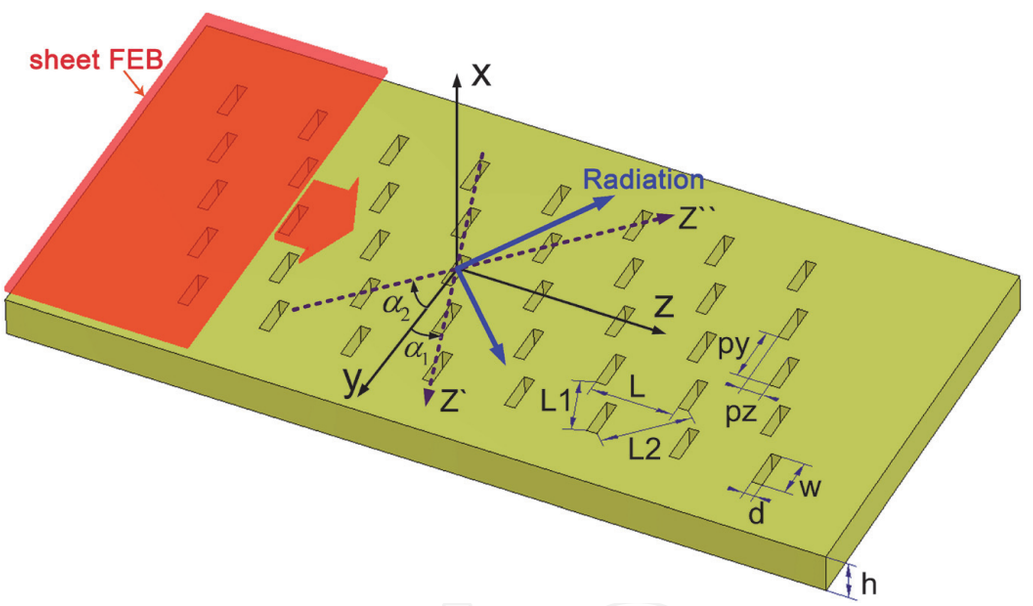

Figure 9.
3D schematic diagram of the sheet free-electron beam driving a 2D SHA.

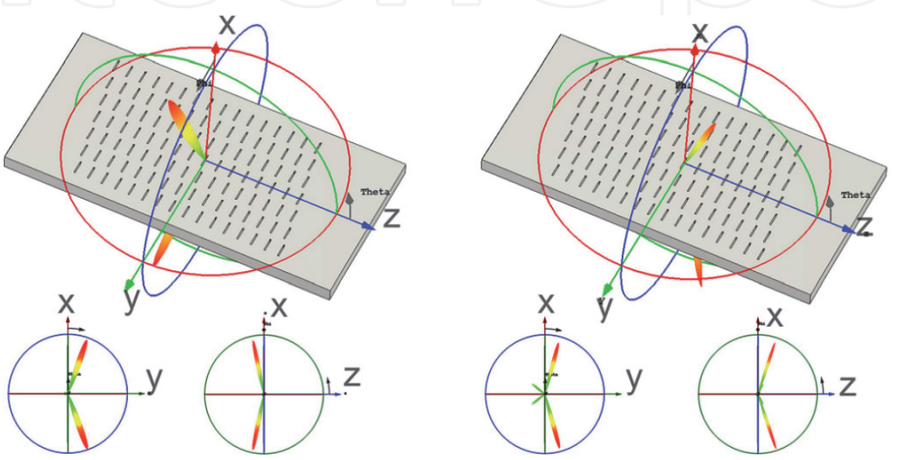

Figure 10.
3D and 2D radiation directivity diagrams of the far-field from a 2D SHA.

developed as radiation sources simultaneously used for several objectives. By rearranging the alignment of SHA, the spatial distribution of CR can also be shaped, which is an increasing hot research topic [35–38].

In addition, we find that, not only S-SPR but also a modified Cherenkov radiation (CR) can be realized from a 2D SHA excited by a sheet FEB, which is illustrated as follows. When a sheet FEB skims over the SHA, the resonant modes within adjacent holes will be successively excited with a time delay of

$$\Delta_t = \frac{L_z}{v_e} = \frac{L}{v_p} \tag{4}$$

in which v_e is the velocity of the FEB in z direction, $v_p = v_e / sin\, \alpha_1$ is the projective (effective) velocity of the FEB in z' direction. The CR in the vacuum can be realized if $v_p > c$, which is exactly the requirement of CR, namely the velocity of the radiation source is greater than the speed of light. Different from that of the transition radiation (TR) [35, 38] and that of the Smith-Purcell radiation (SPR) [36, 37, 39], which are frequency dependent, the spectral and spatial shaping of CR is independent from the frequency, indicating that the radiations of all frequencies are at the same direction.

This CR can be more effectively manipulated and even be focused at specific spots in the space by re-arranging the subwavelength holes in the array. When the subwavelength holes are lined hyperbolically on the conductor plate, the CR will be focused at a specific spot in the space as shown in **Figure 11** [40].

2.3 S-SPR from surface plasmonics

In above S-SPR schemes, the resonator arrays are all realized by perfect electric conductor (PEC). When PEC is replaced by semiconductors or metamaterials with terahertz surface plasmonics (SPs) taken into account, the electromagnetic properties of the rectangular sub-wavelength hole (RSH) will change significantly [41–45]. In this sub-section, we propose to use free-electron beam to excite an array of open resonators covered by an array of meta-films, the schematic diagram of which is shown in **Figure 12**.

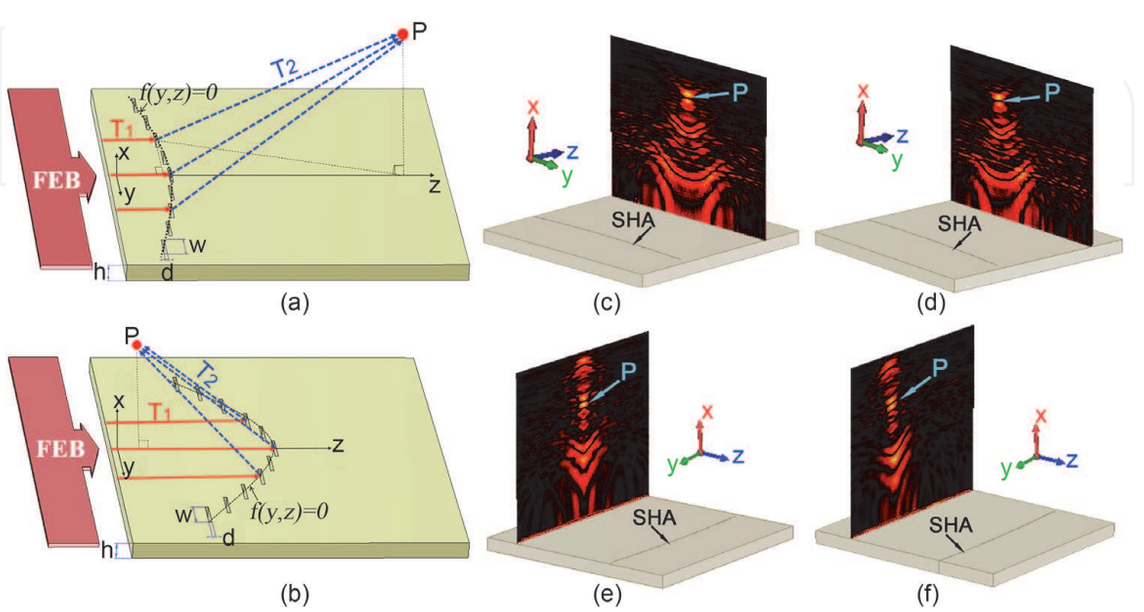

Figure 11.
(a) and (b) The proposed scheme using a sheet FEB to excite a SHA, which is lined along the curve. (c–f) Simulated field intensity distributions in the focusing plane.

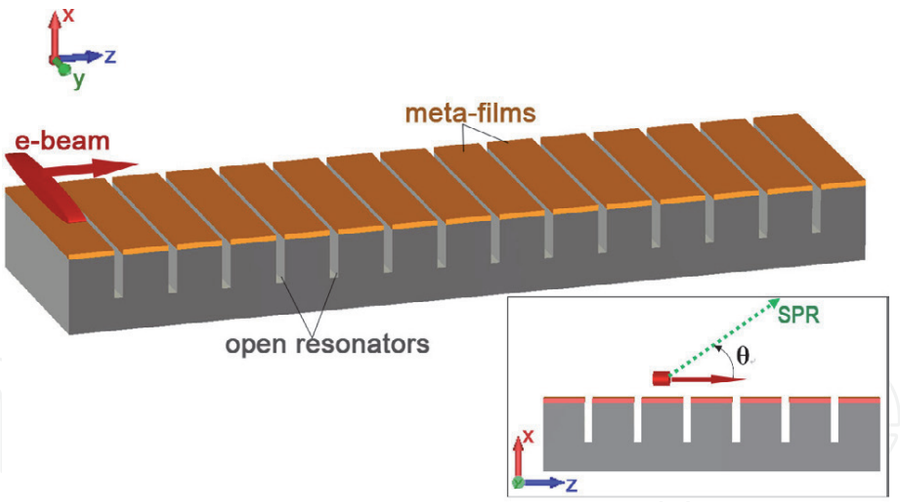

Figure 12.
3D diagram of the proposed scheme and its cross-section (in the inset).

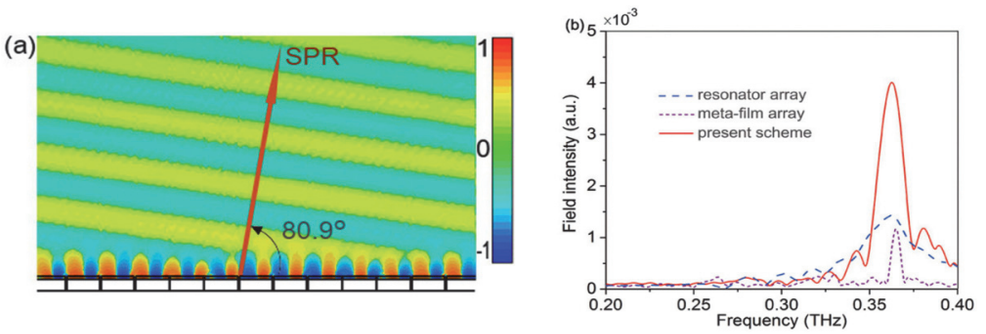

Figure 13.
(a) Simulated field (E_z) contour map. (b) Simulated radiation spectra of three cases.

We find that, when there is only an array of meta-films, the fields are largely confined on the meta-films array, and only a small portion can radiate into the upper space; while there is only open-resonators array, the waves can efficiently radiate into space, however, the surface waves in the open-resonator array is much weaker than that in the meta-films array, so as that the radiation intensity is much weaker. When the open-resonators array and the meta-films array are combined, the FEB first excites the SPs on the meta-films, which then induce the resonator modes within the open-resonators. The SPs are the effective excitation sources for the resonant modes in the open-resonators [46]. When the SPs are coupled with the resonator modes, namely, the resonant frequency of the SPs matches that of the resonator mode, the intensity of the resonator mode, together with the radiation intensity, will be greatly enhanced [47]. **Figure 13** shows that compared with the un-coupled cases, the radiation field intensity of the proposed model is enhanced by more than three times, indicating that the power of radiation will be increased by about an order of magnitude.

3. Terahertz free-electron sources based on S-SPR

In the section, we introduce a class of terahertz free-electron sources based on the mechanism of S-SPR illustrated in Section 2. The schematic diagram of the

proposed source is shown in **Figure 14**. It looks similar to a conventional Orotron, which is an electronic oscillator with open resonator and reflecting grating [48, 49]. A dc electron beam passes over a rectangular grating, from which S-SPR is generated in the perpendicular direction. A planar conductor mirror is placed above the grating, which reflects the radiation waves. The electromagnetic waves then propagate back and forth between the radiation grating and the conductor mirror, forming a series of oscillation modes between them, which is in effect an electromagnetic cavity with open boundary. These oscillation modes will interact with the electron beam and will be amplified via gaining energy from the electron beam. Unlike the conventional Orotron based on O-SPR, here the S-SPR is applied. Since the intensity of S-SPR is remarkably higher than that of O-SPR, the oscillation modes with higher intensity will be excited in the grating-mirror cavity, so as that the output power will be remarkably enhanced.

The distance between the grating and the reflection mirror should be chosen as follows. Since the tangential electric field should reach the maximum at the beam position and vanish at the surface of the conductor mirror, the wavelength of the oscillation waves between the grating and mirror can be evaluated by the equation

$$H \approx \frac{\lambda}{2}\left(p + \frac{1}{2}\right) \tag{5}$$

in which p is a non-negative integer. When the wavelength of the oscillation modes defined by Eq. (5) is close to that of the S-SPR defined by Eq. (1), the oscillation modes will be coupled by S-SPR and be enhanced, which also defines the operation requirement of the proposed device.

The simulated results are shown in **Figure 15**, in which **Figure 15(a)** shows the distribution of the modulated electron beam in the 'x-energy' phasespace. We can see that the beam-to-wave efficiency of the model is over 10%. **Figure 15(b)** shows that the oscillation waves are effectively excited in the cavity, and **Figure 15(c)** illustrates that the frequency of the oscillating field matches that of S-SPR. **Figure 15(d)** shows that the output power of the model reaches 4 W/mm at the frequency of 0.3 THz. The simulated results of the conventional Orotron are also shown for the comparison purpose. We can see that the output power of the proposed model is several orders of magnitude higher than that of conventional Orotron based on O-SPR.

In order to further increase the output power, we propose a double-grating scheme as illustrated in **Figure 16**. Two identical gratings are symmetrically set face

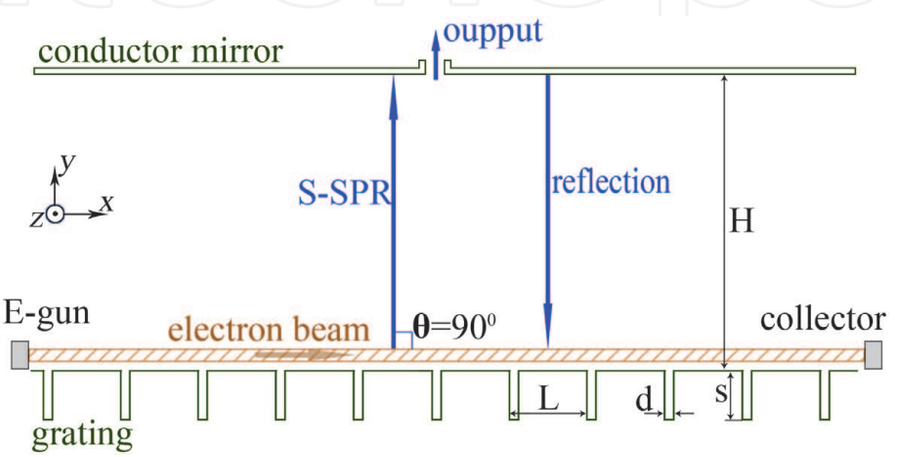

Figure 14.
Diagram of the proposed model of the THz-Orotron based on the S-SPR.

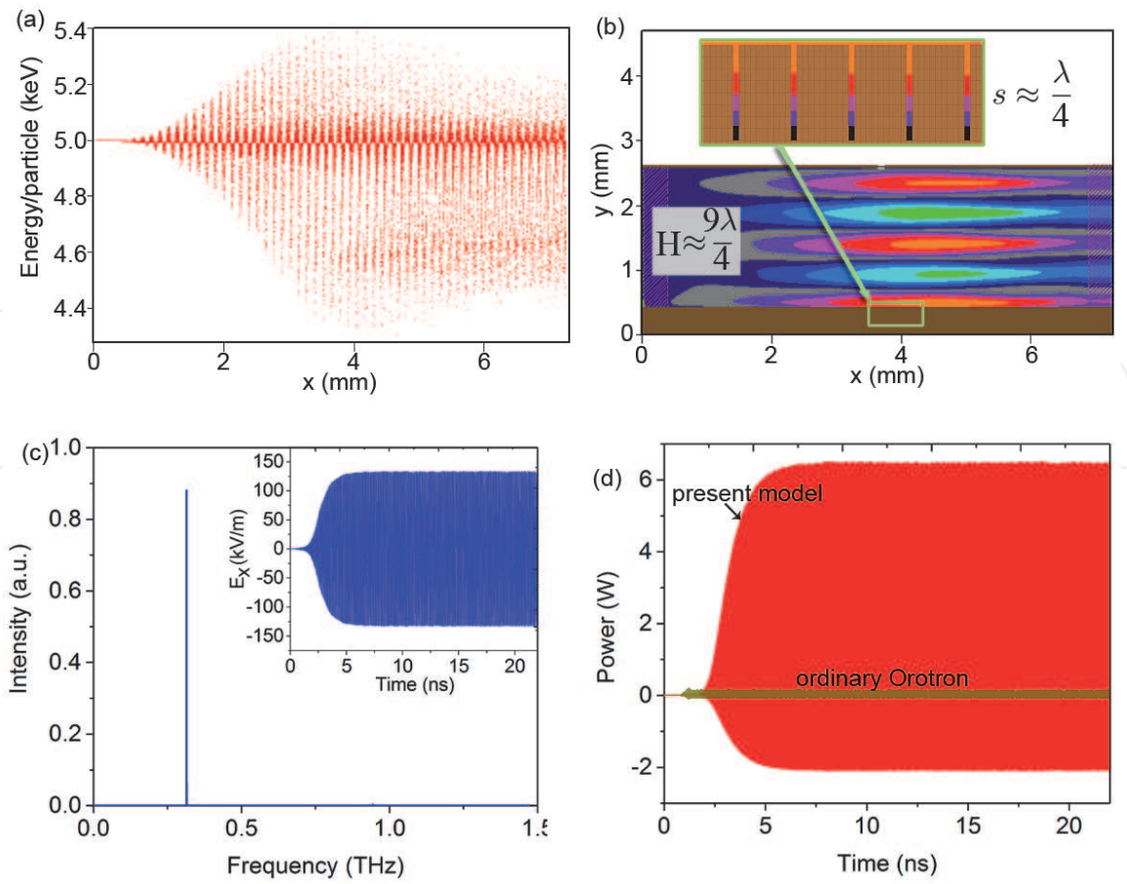

Figure 15.
Simulated snapshot of the phasespace of the modulated electron beam. (b) Simulated contour map of the E_x field. (c) the electric field and its spectrum in the cavity. (d) the output power in the time domain.

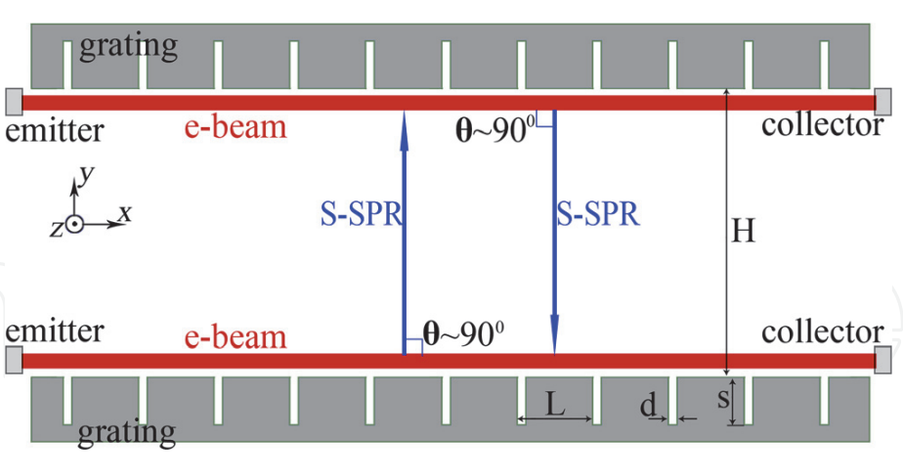

Figure 16.
Schematics of the proposed novel terahertz free-electron laser.

to face, which forms a modified cavity with open boundaries. Two electron beams pass over those gratings, respectively. The S-SPR from each grating are generated in the opposite directions [50], and will interfere in the cavity, forming electromagnetic modes as that in the previous case. Here we appropriately choose grating parameters and the beam velocity, letting the radiation direction of the S-SPR be exactly in the perpendicular direction of the gratings.

Following the analyses of the previous model, the wavelength of the operation modes in the cavity formed by two symmetric gratings can be approximately expressed as:

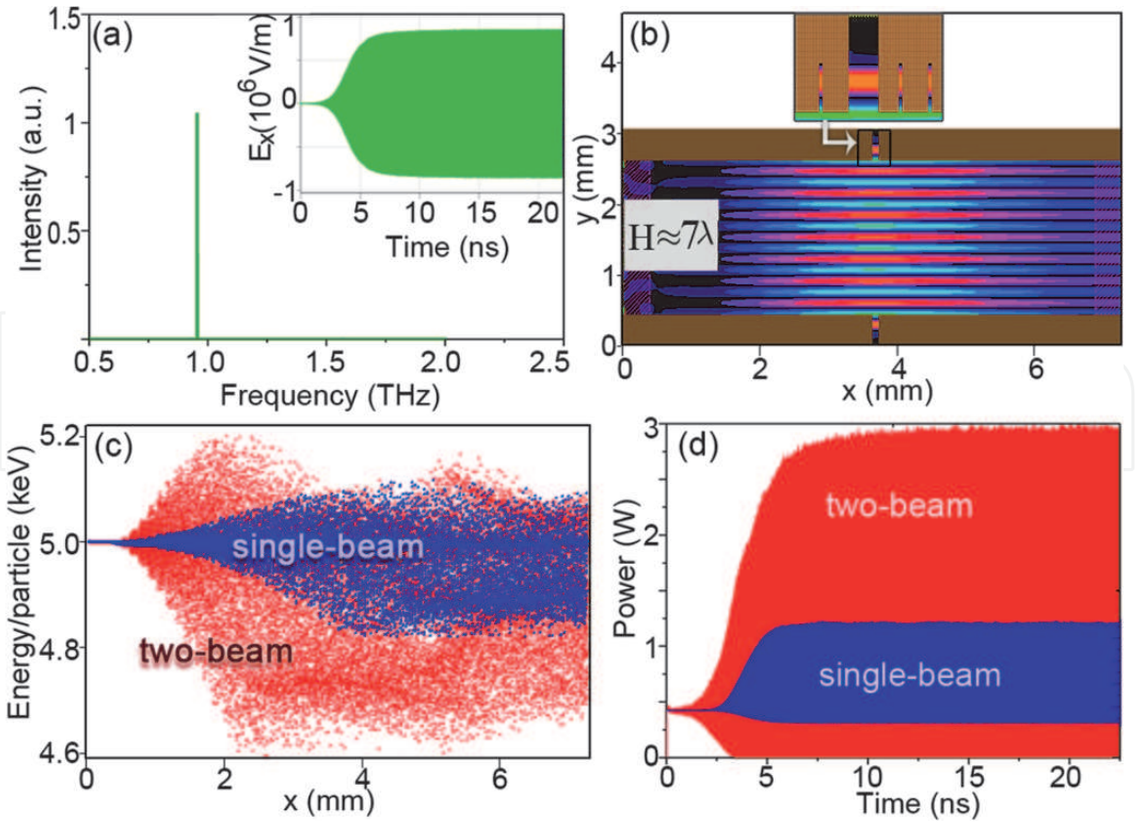

Figure 17.
Simulated results of the proposed terahertz source based on S-SPR (double-beam case). (a) the simulated electric field and its spectrum detected at the port. (b) Snapshot of the contour map of the E_x field. (c) the phase space distributions of the modulated electron beams. (d) Simulated power in the time domain.

$$H \approx p\lambda/2 \tag{6}$$

Figure 17 shows the simulated results of the model, in which the results of the single-beam case is also shown for comparison. One can see that the efficiency and the output power are about 2.5 times than that of the single-beam case. By using an electron beam with moderate current-density (less than 50A/cm^2), the output power reaches 3 watt at the frequency of 0.96 THz. This power level is higher than that of majority terahertz sources in this frequency region, affording a promising option for developing high-power terahertz sources.

4. Conclusions

Using free-electron beams to interact with periodic structures via Smith-Purcell effect is an effective option for developing high-power terahertz sources, which have broad application prospects. In this chapter, we introduced the basic mechanism and several forms of a modified Smith-Purcell radiation–the special Smith-Purcell radiation. Based on the mechanism of the special Smith-Purcell radiation, a set of Smith-Purcell free-electron lasers in the terahertz region were proposed and investigated, promises high-power terahertz wave sources for practical applications.

Acknowledgements

This work was supported by the Natural Science Foundation of China (Grants Nos. 12075239, U1632150, and 61471332).

Conflict of interest

The authors declare no conflicts of interest.

Author details

Weihao Liu[1*], Zijia Yu[2] and Zhi Tao[1]

1 College of Electronic and Information Engineering, Nanjing University of Aeronautics and Astronautics, Nanjing, Jiangsu, China

2 National Synchrotron Radiation Laboratory, University of Science and Technology of China, Hefei, Anhui, China

*Address all correspondence to: liuwhao@nuaa.edu.cn

References

[1] M. Tonouchi. Cutting-Edge Terahertz Technology. Nature Photonics. 2007; 1, 2: 97-105.

[2] C. G. Wade and N. Šibalić, et al. Real-Time Near-Field Terahertz Imaging with Atomic Optical Fluorescence. Nature Photonics. 2017; 11, 1: 40-43.

[3] A. J. Seeds and H. Shams, et al. Terahertz Photonics for Wireless Communications. Journal of Lightwave Technology. 2015; 33, 3: 579-587.

[4] J. H. Booske and R. J. Dobbs, et al. Vacuum Electronic High Power Terahertz Sources. Ieee Transactions On Terahertz Science and Technology. 2011; 1, 1: 54-75.

[5] S. Bielawski and C. Evain, et al. Tunable Narrowband Terahertz Emission From Mastered Laser–Electron Beam Interaction. Nature Physics. 2008; 4, 5: 390-393.

[6] S. J. Smith and E. M. Purcell. Visible Light From Localized Surface Charges Moving Across a Grating. Physical Review. 1953; 92, 4: 1069-1069.

[7] D. Li and Y. Wang, et al. Coherent Radiation at the Fundamental Frequency by a Smith-Purcell Free-Electron Laser with Dielectric Substrate. Applied Physics Letters. 2017; 110, 15.

[8] J. Gardelle and P. Modin, et al. Radiation at 100 and 200 Ghz From a Compact Planar Smith–Purcell Free-Electron Laser. Ieee Transactions On Terahertz Science and Technology. 2017; 7, 2: 151-163.

[9] K. B. Oganesyan. Smith–Purcell Radiation Amplifier. Laser Physics Letters. 2015; 12, 11.

[10] M. Cao and W. Liu, et al. Three-Dimensional Theory of Smith-Purcell Free-Electron Laser with Dielectric Loaded Grating. Journal of Applied Physics. 2014; 116, 10.

[11] J. Gardelle and P. Modin, et al. Observation of Copious Emission at the Fundamental Frequency by a Smith-Purcell Free-Electron Laser with Sidewalls. Applied Physics Letters. 2012; 100, 13.

[12] P. A. Molenaar and P. V. D. Straten, et al. Diagnostic Technique for Zeeman-Compensated Atomic Beam Slowing: Technique and Results. Physical Review a. 1997; 55, 1: 605-614.

[13] M. Castellano and V. A. Verzilov, et al. Measurements of Coherent Diffraction Radiation and its Application for Bunch Length Diagnostics in Particle Accelerators. Physical Review E. 2001; 63, 5.

[14] A. S. Kesar. Smith-Purcell Radiation From a Charge Moving Above a Grating of Finite Length and Width. Physical Review Special Topics Accelerators and Beams. 2010; 13, 2.

[15] M. J. Moran. X-Ray Generation by the Smith-Purcell Effect. Physical Review Letters. 1992; 69, 17: 2523-2526.

[16] W. Liu and Y. Liu, et al. Enhanced Smith–Purcell Radiation by Coupling Surface Plasmons On Meta-Films Array with Resonator Modes On a Grating. Journal of Physics D. 2019; 52, 7.

[17] O. Haeberlé and P. Rullhusen, et al. Calculations of Smith-Purcell Radiation Generated by Electrons of 1-100 Mev. Physical Review E. 1994; 49, 4: 3340-3352.

[18] P. M. V. D. Berg. Smith–Purcell Radiation From a Point Charge Moving Parallel to a Reflection Grating. Journal of the Optical Society of America. 1973; 63, 12: 1588-1597.

[19] D. V. Karlovets and A. P. Potylitsyn. Comparison of Smith-Purcell Radiation Models and Criteria for their Verification. Physical Review Special Topics Accelerators and Beams. 2006; 9, 8.

[20] J. H. Brownell and J. Walsh, et al. Spontaneous Smith-Purcell Radiation Described through Induced Surface Currents. Physical Review E. 1998; 57, 1: 1075-1080.

[21] W. Liu and Y. Lu, et al. A Multimode Terahertz-Orotron with the Special Smith–Purcell Radiation. Applied Physics Letters. 2016; 108, 18.

[22] W. Liu and Z. Xu. Special Smith–Purcell Radiation From an Open Resonator Array. New Journal of Physics. 2014; 16, 7.

[23] W. Liu and L. Sun, et al. Improved Terahertz Smith–Purcell Radiation Using Side-Opening Cylindrical Gratings. Journal of Applied Physics. 2020; 127, 18.

[24] J. Gardelle and L. Courtois, et al. Observation of Coherent Smith-Purcell Radiation Using an Initially Continuous Flat Beam. Physical Review Special Topics Accelerators and Beams. 2009; 12, 11.

[25] J. T. Donohue and J. Gardelle. Simulation of Smith-Purcell Radiation Using a Particle-in-Cell Code. Physical Review Special Topics Accelerators and Beams. 2005; 8, 6.

[26] S. Liu and M. Hu, et al. Electromagnetic Diffraction Radiation of a Subwavelength-Hole Array Excited by an Electron Beam. Physical Review E. 2009; 80, 3: 36602-36602.

[27] H. Liu and A. Yariv. Designing Coupled-Resonator Optical Waveguides Based On High-Q Tapered Grating-Defect Resonators. Optics Express. 2012; 20, 8: 9249-9263.

[28] I. G. Tigelis and J. L. Vomvoridis, et al. High-Frequency Electromagnetic Modes in a Dielectric-Ring Loaded Beam Tunnel. Ieee Transactions On Plasma Science. 1998; 26, 3: 922-930.

[29] W. Li and Y. Liu, et al. Spectrum Discretization of Smith–Purcell Radiation for Efficient Multicolor Terahertz Emission. Journal of Physics D. 2020; 53, 18.

[30] W. Liu and L. Zhang, et al. Coherent Terahertz Emission From Free-Electron-Driven Fabry-Perot Resonators with Coupled Grooves. Journal of Physics D. 2021; 54, 5.

[31] F. J. García-Vidal and L. Martín-Moreno, et al. Light Passing through Subwavelength Apertures. Reviews of Modern Physics. 2010; 82, 1: 729-787.

[32] W. L. Barnes and A. Dereux, et al. Surface Plasmon Subwavelength Optics. Nature. 2003; 424, 6950: 824-830.

[33] H. F. Ghaemi and T. Thio, et al. Surface Plasmons Enhance Optical Transmission through Subwavelength Holes. Physical Review B. 1998; 58, 11: 6779-6782.

[34] L. Liang and W. Liu, et al. Multi-Color and Multidirectional-Steerable Smith-Purcell Radiation From 2D Sub-Wavelength Hole Arrays. Applied Physics Letters. 2018; 113, 1.

[35] B. P. Clarke and K. F. MacDonald, et al. Direction-Division Multiplexed Holographic Free-Electron-Driven Light Sources. Applied Physics Letters. 2018; 112, 2.

[36] R. Remez and N. Shapira, et al. Spectral and Spatial Shaping of Smith-Purcell Radiation. Physical Review a. 2017; 96, 6.

[37] Z. Wang and K. Yao, et al. Manipulating Smith-Purcell Emission

with Babinet Metasurfaces. Physical Review Letters. 2016; 117, 15.

[38] G. Li and B. P. Clarke, et al. Holographic Free-Electron Light Source. Nature Communications. 2016; 7, 1: 13705-13705.

[39] D. Y. Sergeeva and A. A. Tishchenko, et al. Smith-Purcell Radiation From Concave Dotted Gratings. Journal of Instrumentation. 2018; 13, 2.

[40] Y. Liu and W. Liu, et al. Threshold-Less and Focused Cherenkov Radiations Using Sheet Electron-Beams to Drive Sub-Wavelength Hole Arrays. Optics Express. 2018; 26, 26: 34994-35002.

[41] Y. Liu and W. Liu, et al. Efficient and Tunable Terahertz Emission by Transforming Surface Waves to Coherent Smith–Purcell Radiation. Ieee Transactions On Plasma Science. 2021; 49, 1: 455-459.

[42] W. Liu and L. Liang, et al. Two-Dimensional Reversed Cherenkov Radiation On Plasmonic Thin-Film. Optics Express. 2017; 25, 15: 18216-18229.

[43] W. Liu. Dispersive 2D Cherenkov Radiation On a Dielectric Nano-Film. Scientific Reports. 2017; 7, 1: 5787-5787.

[44] W. Liu. Free-Electron Exciting and Steering of the Radiation From Surface Plasmons On Nanowire Array. Ieee Photonics Technology Letters. 2016; 28, 23: 2657-2660.

[45] W. Liu. Coherent and Tunable Light Radiation From Nanoscale Surface Plasmons Array Via an Exotic Smith-Purcell Effect. Optics Letters. 2015; 40, 20: 4579-4582.

[46] S. Liu and P. Zhang, et al. Surface Polariton Cherenkov Light Radiation Source. Physical Review Letters. 2012; 109, 15: 153902-153902.

[47] Z. Yu and Y. Liu, et al. Transforming Terahertz Plasmonics within Subwavelength Hole Arrays Into Enhanced Terahertz Mission Via Smith-Purcell Effect. Optics Express. 2020; 28, 7: 9501-9509.

[48] V. L. Bratman and B. S. Dumesh, et al. Terahertz Orotrons and Oromultipliers. Ieee Transactions On Plasma Science. 2010; 38, 6: 1466-1471.

[49] Y. A. Grishin and M. R. Fuchs, et al. Pulsed Orotron - A New Microwave Source for Submillimeter Pulse High-Field Electron Paramagnetic Resonance Spectroscopy. Review of Scientific Instruments. 2004; 75, 9: 2926-2936.

[50] W. Liu and Y. Lu, et al. A Compact Terahertz Free-Electron Laser with Two Gratings Driven by Two Electron-Beams. Physics of Plasmas. 2017; 24, 2.